Journal of Environmental Chemical Engineering 13 (2025) 118347

Contents lists available at ScienceDirect

Journal of Environmental Chemical Engineering

journal homepage: www.elsevier.com/locate/jece

# Enhanced low-temperature catalytic activity and $SO_2$ resistance in ethane oxidation over Pt-CoZr catalysts: Insights into the promoting effects of Pt and Zr

Ling Wang [a], Beilong Lin [b], Zhiyuan Gong [a], Minghui Tang [a,c,*], Shengyong Lu [a,b,*], Jianhua Yan [a]

[a] State Key Laboratory of Clean Energy Utilization, Zhejiang University, Hangzhou, Zhejiang 310027, China
[b] Taizhou Institute of Zhejiang University, Taizhou, Zhejiang 318012, China
[c] Qingshanhu Energy Research Center, Zhejiang University, Qingshanhu Science and Technology City, 1699 Dayuan Road, Hangzhou, Zhejiang 311305, China

ARTICLE INFO

*Keywords:*
Pt-based catalysts
Ethane oxidation
$SO_2$ resistance
Surface acidity
Surface-active oxygen
C-C cleavage

ABSTRACT

Excellent low-temperature catalytic activity and $SO_2$ resistance are two longstanding challenges for existing catalysts in short-chain alkanes oxidation. In this study, superior catalytic activity and stability for ethane degradation on $Co_3O_4$ catalysts were achieved by the introduction of Pt and Zr. Especially, the 0.5 %Pt-CoZr catalyst demonstrated exceptional catalytic performances with the complete conversion of ethane at 275 °C. Additionally, the 0.5 %Pt-CoZr catalyst exhibited flexible adaptability to complex working conditions and showed outstanding stability in the presence of $H_2O$ and $SO_2$. The enhanced redox property was obtained by the interaction between Pt and Co, which significantly improved the low-temperature catalytic efficiency. The 0.5 % Pt adding into CoZr led to the weaken Co-O bond strength and more oxygen vacancies, which contributed to the electron transfer into O atoms and finally generated more surface-active oxygen. Thus, the cleavage of the C-C bond was facilitated in 0.5 %Pt-CoZr catalyst, ultimately accelerating the degradation process of the acetate into formate. Meanwhile, the dopant of Zr greatly increased the specific surface area of catalysts and promoted the distribution of Pt particles. Moreover, the enhanced sulfur resistance was achieved by the increased weak acid sites with Zr doping, which effectively inhibited $SO_2$ adsorption and sulfates deposition. Therefore, the present study revealed the underlying structure-activity mechanism of ethane oxidation process and offered an efficient catalyst for ethane degradation with high-performance $SO_2$ tolerance.

## 1. Introduction

Environment pollution is one of the urgent challenges in the society and the massive emission of volatile organic compounds (VOCs) has made great threats to the environmental and humans [1]. Among them, short chain alkanes are a typical category of the most intractable VOCs to be eliminated owing to the stable molecule structure of C-H bonds [2]. Especially, ethane ($C_2H_6$) accounts for a large proportion of alkane emissions of various sources including vehicle emission, petrochemical processing and coal chemical industry, which causes serious atmospheric problems [3,4]. Catalytic oxidation has been widely investigated for the VOCs control for its low energy consumption, high degradation efficiency and non-secondary pollution [5]. Supported noble metals (Pt, Pd, and Ru) and transition metal oxides ($Co_3O_4$, $CeO_2$, and $MnO_2$) are widely applied in catalytic reactions and both are reported to present excellent low-temperature performances [6–11]. However, despite the high activity, the inevitable and realistic problems (impurities and harsh conditions) seriously hinder the application of catalysts [12,13]. Among them, $SO_2$ exists widely in industrial exhaust gases and has been highly valued, which can interact with the active metals to form metallic sulfates and finally leads to the deactivation of the catalysts as well as the suppressing catalytic reaction [14]. Up to now, the design of highly active and strongly $SO_2$-resistance catalysts is still a tough breakthrough which needs to be conquered.

$Co_3O_4$-based is known to be favorable for the activation of the C-H bond and has been widely used for the degradation of short-chain alkanes [15]. But the $Co_3O_4$ surface was reported to be easily poisoned by the $SO_2$ to change into inactive cobalt sulfate species and finally

* Corresponding authors at: State Key Laboratory of Clean Energy Utilization, Zhejiang University, Hangzhou, Zhejiang 310027, China.
*E-mail addresses:* lytmh1214@zju.edu.cn (M. Tang), lushy@zju.edu.cn (S. Lu).

https://doi.org/10.1016/j.jece.2025.118347
Received 9 May 2025; Received in revised form 17 July 2025; Accepted 28 July 2025
Available online 28 July 2025

deactivate [16]. Nowadays, great efforts in introducing modified components (Fe, Cu, V etc.) had been done to enhance the poisoning tolerance of selective catalytic reduction(SCR) catalysts and were reported to be effective [17–20]. For example, Zha et al. confirmed that Fe species could keep the strong adsorption of $SO_2$ from active Co oxides and inhibit the formation of stable sulfate species, which effectively reduced the effects of $SO_2$ poisoning [21]. Meanwhile, Cu was reported to show great the resistance of $SO_2$ owing to the effective inhibition of the adsorption and further oxidation of $SO_2$ [22,23]. In addition, the effects of V-doped catalysts on the enhanced sulfur resistance were determined by the increased surface acidity and the restrain the deposition of sulfate species [20,24]. Wu et al. successfully prepared a hollow core-shell structure $CoNiO_x$@$Cu_5V_1O_x$ catalyst with excellent catalytic activity and sulfur tolerance for the catalytic combustion of $C_3H_8$, in which the $Cu_5V_1O_x$ shell layer effectively inhibited the adsorption toxicity of $SO_2$ at the $Co^{3+}$ site [25]. However, there were few reports on the development of efficient catalysts with $SO_2$ tolerance for catalytic degradation of ethane in coal processing industry, and more attention should be paid on the studies of the structure-activity relationship and $SO_2$ tolerance mechanism as well.

Especially, $ZrO_2$ was extensively applied as support or dopant for various catalysts because of its excellent structural stability and chemical resistance [26–28]. It was reported that 1 % Zr doped $Co_3O_4$ catalysts showed improved performances on propane oxidation than original $Co_3O_4$ catalyst [28]. Meanwhile, Zeng and co-workers investigated that higher catalytic activity for propane oxidation could be obtained by more addition of Zr in $MnZrO_x$ oxides owing to the superior reducibility, oxygen mobility and the higher specific surface area [29]. Besides, Wu et al. further carried out related DFT theoretical calculations and proved that the presence of Zr doping in $Mn_1Zr_xO_y$ catalysts reduced the formation energy of oxygen vacancy and led to higher concentration of oxygen vacancies, which played a decisive role in propane catalytic oxidation [30]. More importantly, it had been declared that the doping of Zr in La-Mn perovskite oxides enhanced the surface acidity of catalysts, inhibited the adsorption of $SO_2$, and thereby improved the $SO_2$ resistance of the catalyst [31]. Therefore, we envisioned that the Zr doped in $Co_3O_4$ oxides would not only improve the oxidation activity of ethane combustion but also enhance the stability while exposing to $SO_2$.

Herein, a series of $Co_xZr_{10-x}$ mixed oxides were prepared by a simple sol-gel method. Meanwhile, to achieve efficient oxidation under low-temperature, noble metal Pt was added into the catalysts via an incipient wetness impregnation. Experimental results showed that 0.5 %Pt-CoZr catalyst achieved the complete conversion of ethane at 275 °C and presented satisfactory stability under different conditions (long-term, humid atmosphere, and temperature-alternating tests). Based on the analysis of the characterizations, the presence of Pt significantly enhanced the redox property of $Co_xZr_{10-x}$ catalysts, which played the decisive role in the catalytic activity. Meanwhile, the introducing of Zr would enlarge the surface area, increase the active surface oxygen species and create more oxygen vacancies on the catalysts, which consequently contributed to the catalytic stability and the sulfur resistance. Specifically, in contrast to the rapid deactivation of 0.5 %Pt-$Co_3O_4$ catalyst, 0.5 %Pt-CoZr could obtain high conversion efficiency of ethane above 80 % after the 480-min exposure to 50 ppm $SO_2$. Consequently, the corresponding reaction mechanism, degradation path, and $SO_2$ tolerance mechanism of ethane oxidation were further elucidated in this study.

## 2. Experimental section

### 2.1. Synthesis of catalysts

The catalysts were all synthesized by a sol-gel method. Typically, a certain amount of cobalt nitrate and zirconium nitrate was dissolved in 20 mL deionized water to form a clear solution, while 0.15 mol citric acid was added into 15 mL deionized water. Then, the citric acid solution was immersed dropwise into the above metallic solution under magnetic stirring at 60 °C for 1 h. Next, the mixture was evaporated overnight at 80 °C. The obtained solid was grinded and transferred into a muffle furnace. The heating process followed as 300 °C for 1 h and then 350 °C for 4 h under air condition with the heating rate of 5 °C·min$^{-1}$. The obtained samples were labeled as $Co_xZr_{10-x}$(x represented the molar ratio of Co in the whole catalyst). Among them, the $Co_9Zr_1$ catalyst was abbreviated as CoZr particularly.

Subsequently, a series of Pt catalysts supported on $Co_3O_4$ and $Co_xZr_{10-x}$ were synthesized by wetness impregnation using Pt$(NH_3)_4(NO_3)_2$ solution as precursor. A desired amount of Pt$(NH_3)_4(NO_3)_2$ solution was dissolved in 1 g $Co_3O_4$ and $Co_xZr_{10-x}$ catalysts under continuous stirring. After impregnation, the samples were dried at 90 °C in a drying oven overnight and calcined at 300 °C for 3 h in air. Finally, the catalysts were treated at 300 °C with 10 %$H_2$/Ar for 1 h. Pt was deposited on $Co_9Zr_1$ and $Co_3O_4$ supports with a nominal Pt loading of 0.5 wt% and denoted as 0.5 %Pt-CoZr and 0.5 %Pt-$Co_3O_4$, respectively.

### 2.2. Catalyst characterization

The catalysts were characterized by techniques as followed: X-ray diffraction (XRD), Brunauer-Emmett-Teller (BET), scanning electron microscopy (SEM), transmission electron microscopy (TEM), X-ray photoelectron spectroscopy (XPS), electron paramagnetic resonance (EPR), $H_2$ temperature-programmed reduction ($H_2$-TPR), $O_2$ temperature-programmed desorption ($O_2$-TPD), inductively coupled plasma optical emission spectroscopy (ICP-OES), Raman spectra, in situ diffuse reflectance infrared Fourier transform spectroscopy (in situ DRIFTs). And the details were provided in the Supporting information.

### 2.3. Catalytic activity

The catalytic performance of the catalysts for ethane oxidation was tested in a fixed-bed reactor at atmospheric pressure. To eliminate the hot spots effect, the prepared catalyst (100 mg) was diluted in 100 mg of quartz sand (40–60 mesh) and then was placed in the tubular reactor. The reactant gas was composed of 0.2 vol% $C_2H_6$, 21 vol% $O_2$ (5 or 10 vol% $H_2O$, 50 ppm $SO_2$, while used) and $N_2$ balance, with a total flow rate of 50 mL·min$^{-1}$, corresponding to a WHSV of 30,000 mL·g$^{-1}$·h$^{-1}$. The reactants and products were analyzed using a gas chromatograph (GC-9790II FuLi) equipped with a hydrogen flame ionization detector (FID) and a thermal conductivity detector (TCD, for $CO_2$ and CO detection). Analyses were made at each temperature until steady state activity was attained (stabilized 30 min before the analysis). The conversion of ethane ($X_{C2H6}$) and the yield of $CO_2$ ($Y_{CO2}$) were calculated as followed:

$$X_{C2H6} = \frac{[C_2H_6]_{in} - [C_2H_6]_{out}}{[C_2H_6]_{in}} \times 100\%$$

$$Y_{CO2} = \frac{[CO_2]_{out}}{2 \times [C_2H_6]_{in}}$$

Where $[C_2H_6]_{in}$ and $[C_2H_6]_{out}$ are the inlet and outlet concentrations of ethane, respectively. $[CO_2]_{out}$ is the outlet concentration of $CO_2$ after reaction.

The further reaction evaluation was provided in Supporting information.

## 3. Results and discussions

### 3.1. Catalytic performances of prepared catalysts

The ethane catalytic activity of the synthesized catalysts as functions of reaction temperature was evaluated under the same conditions, and the temperatures corresponding to the 50 % and 90 % conversion of

ethane (denoted as $T_{50}$ and $T_{90}$) were listed in Table 1. Generally, $Co_3O_4$ showed satisfactory activity for ethane oxidation, but the $ZrO_2$ was inactive in the whole temperature region. Typically, as displayed in Fig. S1a, 10 % Zr introduced into the $Co_3O_4$ catalysts exhibited an enhanced activity than single metal catalysts. Thus, the $Co_9Zr_1$ catalysts (denoted as CoZr) was selected as the target catalyst for supporting noble metal Pt, which was also optimized by regulating the roasting temperature showed in Fig. S1b. Moreover, the optimal adding content of Pt in CoZr catalyst was determined at 0.5 wt% as showed in Fig. S2a. Based on the above results, we carried out the following detailed experiments to show the effects of Pt and Zr on the $Co_3O_4$ catalysts. As displayed in Fig. 1a, the catalytic activities of the catalysts for ethane oxidation decreased in the order of 0.5 %Pt-CoZr> 0.5 %Pt-$Co_3O_4$>CoZr>$Co_3O_4$>$ZrO_2$. Moreover, we carried out a three-time repetitive experiments of ethane oxidation between 0.5 %Pt-CoZr and 0.5 %Pt-$Co_3O_4$ catalysts in Fig. S3, which further confirmed the improved activity of 0.5 %Pt-CoZr catalyst. Meanwhile, the $CO_2$ selectivity of tested catalysts was also depicted in Fig. S4. The $T_{90}$ over 0.5 % Pt-CoZr catalyst was achieved at 247 °C, lower than that of 0.5 %Pt-$Co_3O_4$ (262 °C) and CoZr (272 °C) catalysts, which was superior to most reported catalysts (Fig. 1b and Table S1). Besides, the kinetic studies of catalysts were displayed in Fig. 1c, and the apparent activation energy (Ea) of 0.5 %Pt-CoZr showed the lowest value (63.64 kJ/mol) compared with that of 0.5 %Pt-$Co_3O_4$ (64.17 kJ/mol), CoZr (78.26 kJ/mol) and $Co_3O_4$ (103.52 kJ/mol) catalysts. Moreover, considering the fluctuating flow conditions presented in actual flue gas, the effect of WHSV on the ethane degradation over 0.5 %Pt-CoZr catalyst was further carried out in Fig. S5, and the complete degradation was achieved at 325 °C even under 90000 $mL{\cdot}h^{-1}{\cdot}g_{cat}^{-1}$.

The stability of the catalysts is another crucial factor judging their catalytic performances. As showed in Fig. 1d, the 0.5 %Pt-CoZr catalyst maintained excellent stability under temperature fluctuation impact conditions. Considering the presence of the impurities in the real exhaust condition, the effects $H_2O$ and $SO_2$ on the catalytic stability of prepared catalysts were studies at 275 °C. As depicted in Fig. 1e, the 0.5 %Pt-CoZr catalyst was still able to maintain over 90 % ethane conversion in the impact of water, demonstrating its superior water resistance stability compared to other catalysts (Fig. S5). The effect of $SO_2$ on the catalytic activity was also analyzed. As shown in Fig. 1f, the 0.5 %Pt-CoZr catalyst kept a stable conversion over 80 % of ethane compared to other catalysts, indicating the fantastic stability against $SO_2$. Meanwhile, the improved sulfur resistance was further verified on Pt-CoZr catalyst with different loading contents of Pt in Fig. S2b. It was noteworthy that both $Co_3O_4$ and 0.5 %Pt-$Co_3O_4$ rapidly deactivated within 360 min under the influence of $SO_2$. However, the sulfur resistance of the catalysts was significantly enhanced after the addition of Zr as a promoter, as observed in CoZr and 0.5 %Pt-CoZr. This clearly indicated that Zr played a crucial role in improving the sulfur resistance of the catalysts. The above results demonstrated that 0.5 %Pt-CoZr exhibited excellent ethane conversion performance and stability compared to $Co_3O_4$, showing promising potential for industrial applications. The roles of Pt and Zr in the structure-activity relationship was comprehensive analyzed in the following parts.

### 3.2. Physical properties of catalysts

HRTEM was used for insight into the texture morphology and lattice structure of 0.5 %Pt-CoZr and 0.5 %Pt-$Co_3O_4$ catalysts in Fig. 2. Obviously, smaller and more regular particles were detected in 0.5 %Pt-CoZr catalyst (Fig. 2a) while comparing with 0.5 %Pt-$Co_3O_4$ catalyst (Fig. 2d). Meanwhile, the deposition of Pt nanoparticles was further investigated and the measured d-spacing of 0.23 nm was assigned to the (111) facets of Pt nanoparticles on both catalysts in Fig. 2b and e. Moreover, the texture and morphology of catalysts and the distribution of Pt species were characterized by HAADF. As displayed in Figs. 2c and 2f, smaller Pt nanoparticles were observed on the surface of 0.5 %Pt-CoZr compared to 0.5 %Pt-$Co_3O_4$, which was likely attributed to the addition of Zr promoting the dispersion of Pt on the catalyst surface. The higher metal dispersion determined by the CO pulse chemisorption further confirmed the smaller Pt nanoparticles in the 0.5 %Pt-CoZr catalyst. Moreover, the result of EDS elemental mapping indicated that the Zr and Pt were successfully loaded and highly dispersed on the surface of 0.5 %Pt-CoZr catalyst (Fig. S7). Besides, we conducted the TEM and HAADF analysis on the used 0.5 %Pt-CoZr catalysts after the catalytic activity test and displayed the results in the Fig. S8. The results showed that Pt species on used 0.5 %Pt-CoZr catalyst was in highly dispersed state without obvious aggregation even after the high-temperature reaction, indicating the excellent stability of 0.5 %Pt-CoZr catalyst in propane oxidation.

The XRD patterns of various samples were studied as shown in Fig. 3a. The prepared $Co_3O_4$ catalyst matched well with the spinel $Co_3O_4$ crystal phase (JCPDS42–1467), while the $ZrO_2$ catalysts showed the phase of $ZrO_2$ (JCPDS49–1642). After introducing the Pt or Zr into the $Co_3O_4$ catalyst, only a slightly evident peak at 36.9° was observed on 0.5 %Pt-CoZr, which was attributed to the (311) crystal planes of $Co_3O_4$ (Fig. S9). Moreover, no characteristic diffraction peaks assigned to Pt metal were recorded owing to a low Pt loading (0.5 wt%) or high dispersion of Pt on the surface of catalysts. Besides, another peak belonged to the crystal phase of CoO was detected in 0.5 %Pt-$Co_3O_4$ catalyst attributed to the reduction of $H_2$ during the preparing process. However, related peak was not discovered in 0.5 %Pt-CoZr catalyst, which was probably contributed to the influence of Zr [30].

The specific surface area and pore structure parameters of the prepared materials were characterized by low-temperature $N_2$ adsorption, showed in Fig. 3b and Table 1. It was obvious that all prepared catalysts displayed the unique IV-type isotherms with irregular appearance. In detail, 0.5 %Pt-CoZr and CoZr catalysts possessed a type IV isotherm with a H3 type hysteresis loop, but other belonged to a H4-type. Furthermore, the surface area of them followed the order of 0.5 %Pt-CoZr (79.4 $m^2/g$)>CoZr (72.9 $m^2/g$)>$ZrO_2$ (22.9 $m^2/g$)> 0.5 %Pt-$Co_3O_4$ (19.1 $m^2/g$)>$Co_3O_4$ (11.5 $m^2/g$). The results indicated that the introduction of Zr made great contribution to the high surface areas.

**Table 1**
Catalytic activities, pore structure and surface information of the catalysts.

| Catalyst | $T_{50}$ (°C) | $T_{90}$ (°C) | Rate[a] ($mol{\bullet}g^{-1}{\bullet}s^{-1}$) | $S_{BET}$[b] ($m^2/g$) | $V_t$[c] ($cm^3/g$) | $D_p$[d] (nm) | Binding energy(eV) | | | | |
|---|---|---|---|---|---|---|---|---|---|---|---|
| | | | | | | | $Co^{3+}$ $2p_{1/2}$ | $Co^{2+}$ $2p_{1/2}$ | $O_{OH}$ | $O_{surf}$ | $O_{latt}$ |
| $ZrO_2$ | > 300 | - | - | 22.9 | 0.03 | 5.5 | - | - | 532.98 | 531.13 | 529.34 |
| CoZr | 232 | 271 | 0.11 | 72.9 | 0.13 | 7.3 | 794.78 | 796.20 | 532.00 | 530.84 | 529.70 |
| 0.5 %Pt-CoZr | 212 | 247 | 0.18 | 79.4 | 0.13 | 6.6 | 794.87 | 796.42 | 531.91 | 530.77 | 529.76 |
| 0.5 %Pt-$Co_3O_4$ | 225 | 260 | 0.15 | 19.1 | 0.12 | 25.3 | 794.84 | 796.43 | 532.22 | 531.09 | 529.83 |
| $Co_3O_4$ | 247 | 279 | 0.04 | 11.5 | 0.12 | 42.6 | 794.80 | 796.19 | 532.24 | 531.26 | 530.00 |

[a] Calculated at 125 °C;
[b] $S_{BET}$: specific surface area obtained by the Brunauer-Emmett-Teller method;
[c] $V_t$: the total of pore volume calculated by BJH desorption method;
[d] $D_p$: the average pore diameter obtained by BJH desorption average pore diameter.

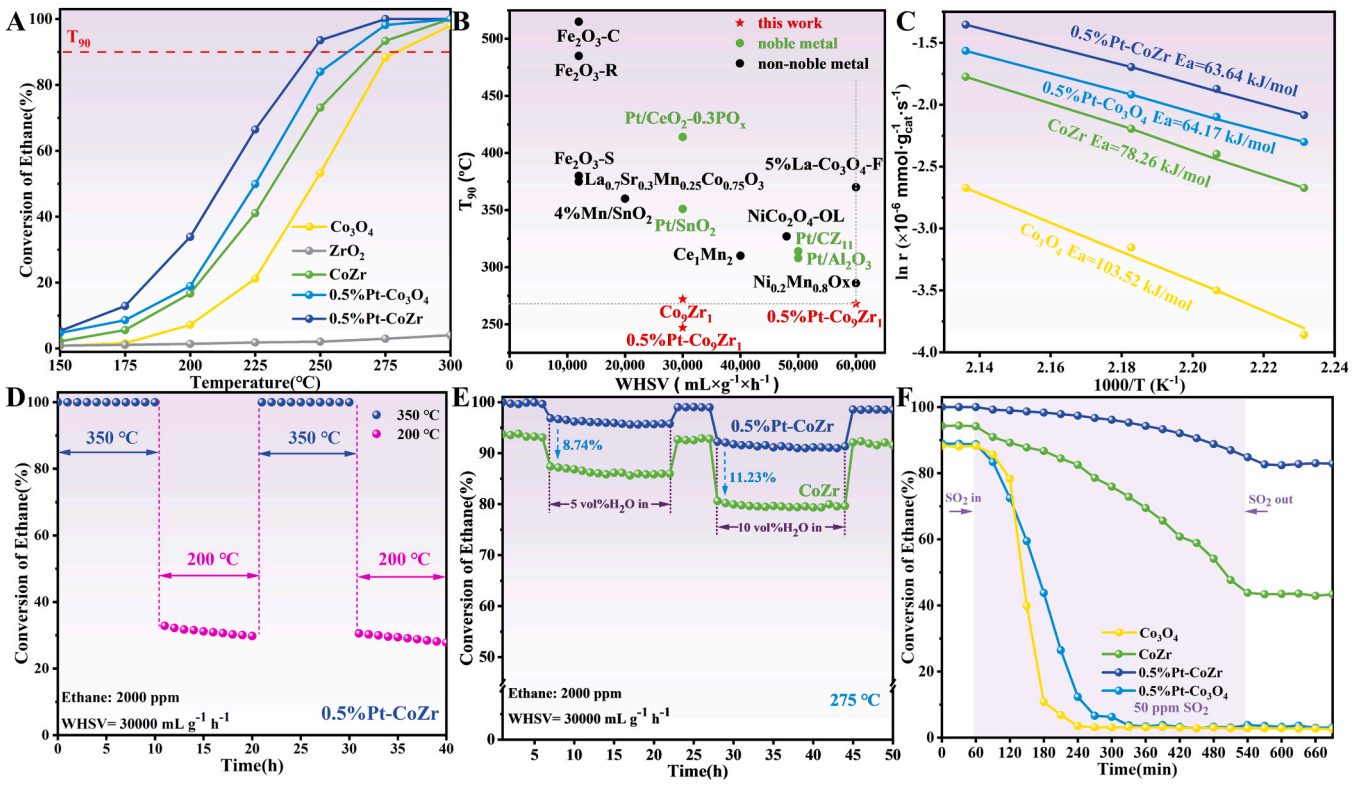


**Fig. 1.** Catalytic performance for ethane oxidation (a), comparation of ethane conversion of $T_{90}$ with other catalysts reported in the literatures (b), arrhenius plots over the prepared catalysts (c), ethane oxidation when alternating the reaction temperature between 200 and 350 °C on the 0.5 %Pt-CoZr catalyst (d), water vapor resistance (5 vol% and 10 vol%) tests for CoZr and 0.5 %Pt-CoZr catalyst at 275 °C (e) and time-varying ethane conversion over catalysts at 275 °C when 50 ppm $SO_2$ was introduced (f). The feed gas consisted of 2000 ppm $C_2H_6$, 21 % $O_2/N_2$, the WHSV was 30,000 mL·h$^{-1}$·g$_{cat}^{-1}$.

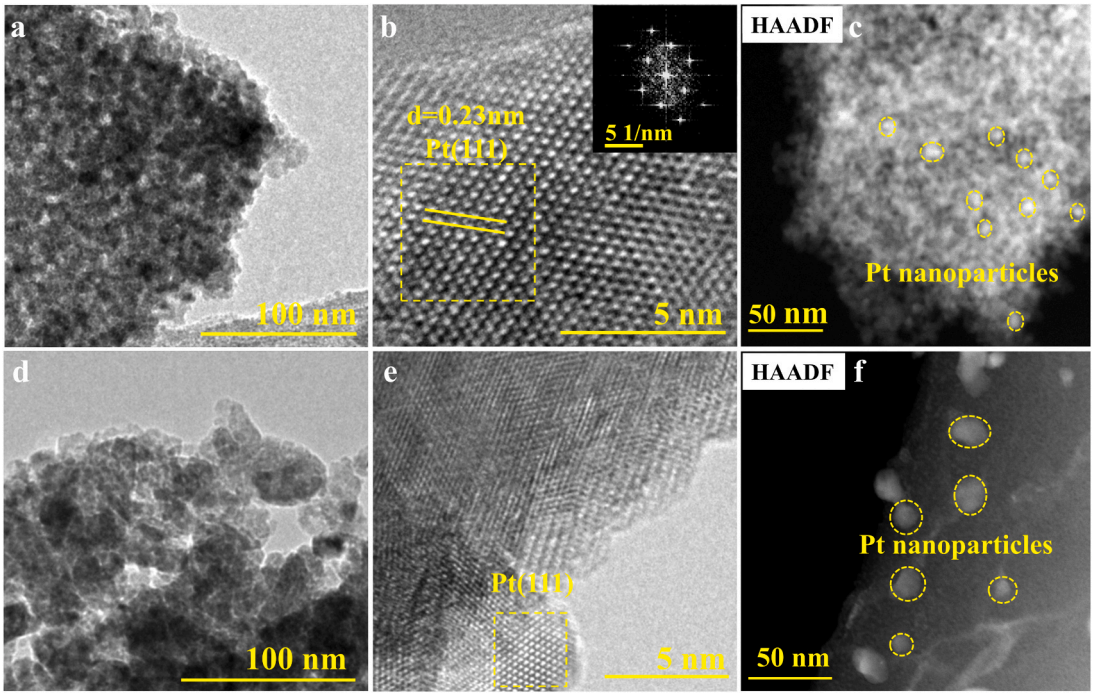


**Fig. 2.** Typical HRTEM and HAADF images of 0.5 %Pt-CoZr catalyst (a-c) and 0.5 %Pt-$Co_3O_4$ catalyst (d-f).

Meanwhile, the similar information of $Co_xZr_y$ catalysts was displayed in the Fig. 3c and further confirmed the critical effects of Zr on the enhancement of surface area. The high specific surface area of 0.5 %Pt-CoZr facilitated the molecular mass transfer and exposed more active sites, thereby demonstrating superior catalytic performance in ethane conversion [32].

As showed in Fig. 3d, four Raman bands at ca. 192, 484, 522 and 689 cm$^{-1}$ were detected and corresponded to $F_{2\,g}^1$, $E_g$, $F_{2\,g}^2$, and $A_{1\,g}$

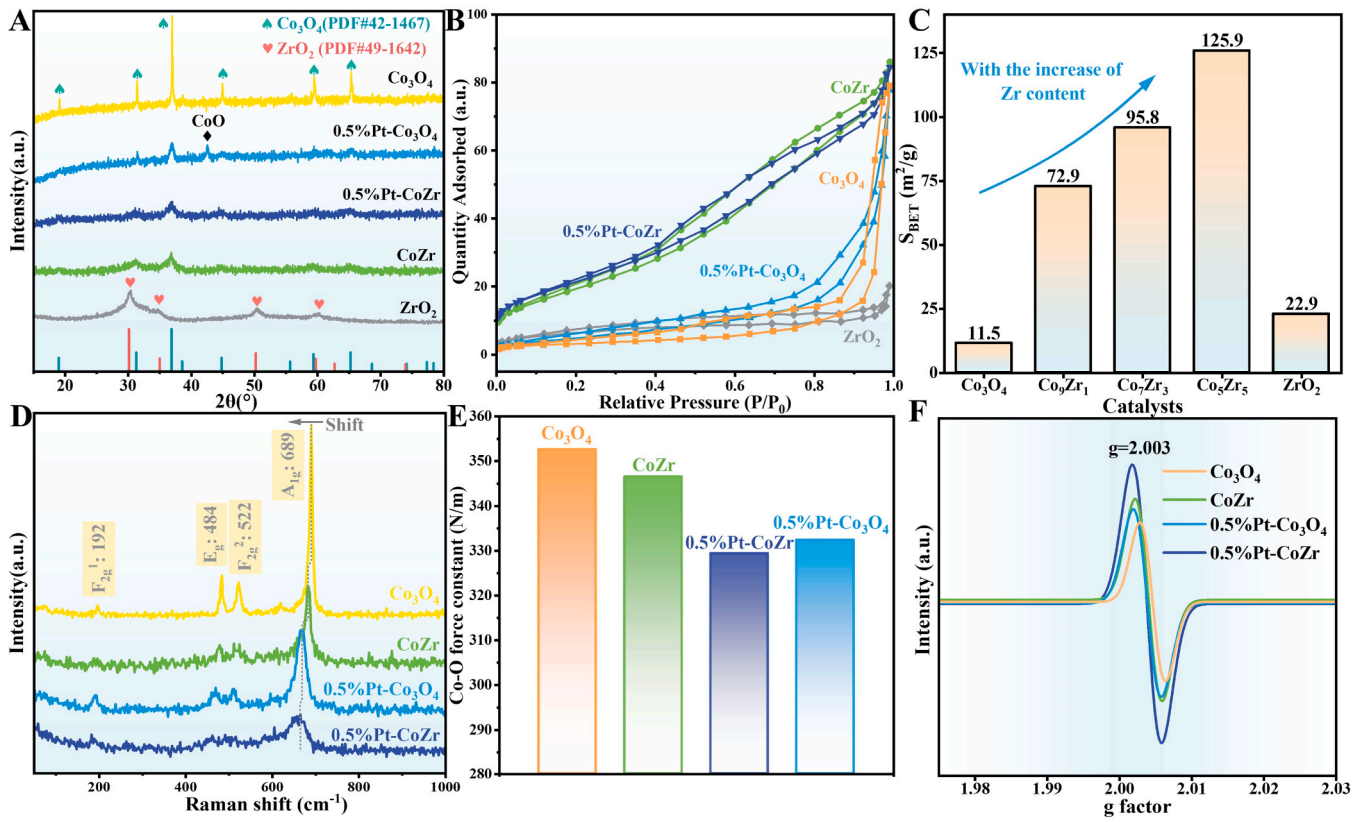


**Fig. 3.** XRD patterns (a), $N_2$ sorption isotherm (b), BET surface area (c), Raman spectra (d), Co-O force constant (e) and EPR spectra (f) of prepared catalysts.

modes of $Co_3O_4$, respectively [33]. Compared to the pure $Co_3O_4$ catalyst, the introduction of Zr and Pt led to a slight shift of the Raman peaks toward lower wavenumbers in CoZr, 0.5 %Pt-$Co_3O_4$, and 0.5 %Pt-CoZr catalysts. These findings suggested modifications in the Co-O bond strength and an enhanced presence of defects. Besides, the bond force constant was calculated to further study the Co-O bond strength according to the Hooke's law [34]:

$$\omega = \frac{1}{2\pi c}\sqrt{k/\mu}$$

where ω, c and μ represented the Raman shift ($cm^{-1}$) of $A_{1\,g}$ symmetry, light velocity ($3.0 \times 10^8$ m/s) and effective mass, respectively. As displayed in Fig. 3e, the Co-O bond force constant (k) followed the order of $Co_3O_4$>CoZr> 0.5 %Pt-$Co_3O_4$> 0.5 %Pt-CoZr, which was exactly opposite to the catalytic activity. The 0.5 %Pt-CoZr catalyst exhibited the lowest Co-O bond strength, indicating that the Co-O bond was more prone to cleavage. This facilitated the participation of oxygen atoms in catalytic reactions and promoted the formation of a large number of oxygen vacancies on the surface of 0.5 %Pt-CoZr [35]. Similar phenomena were also observed in the result of EPR. As displayed in Fig. 3f, the modified catalysts exhibited enhanced peak intensity at the g-value of 2.003 compared to the $Co_3O_4$ catalyst. Especially, 0.5 %Pt-CoZr catalyst demonstrated the strongest symmetric signal, which referred to the abundant electrons trapped in the oxygen vacancy defects [36]. These above results illustrated that the introduction of Zr and Pt weakened the Co-O bonds in $Co_3O_4$ through the interactions among Pt, Zr, and Co. The more oxygen vacancy defects were easier to form in 0.5 %Pt-CoZr catalyst and finally contributed to the promoted catalytic activity. Furthermore, compared to Zr, the introduction of Pt demonstrated a significantly greater capacity to weaken the Co-O bonds in $Co_3O_4$ through metal-metal and metal-oxygen interactions (Fig. 3e).

### 3.3. Structure-activity relationships

XPS was conducted to characterize the valence state changes and surface chemical states. The XPS survey spectra was concluded in Fig. S10, and the Co 2p, O 1 s and Pt 4 f spectra were shown in Fig. 4. The Co 2p XPS profiles of the catalysts could be split into four peaks of $Co^{3+}$ (780.0 eV and 795.0 eV) and $Co^{2+}$ (781.5 eV and 796.5 eV), respectively [15]. Especially, after the introduction of Pt, the binding energies of $Co^{3+}$ shifted to higher values, indicating the presence of electron transfer in $Co_3O_4$ phase. Besides, the ratio of $Co^{3+}/Co^{2+}$ was calculated and followed the order as 0.5 %Pt-CoZr(1.38)> 0.5 %Pt-$Co_3O_4$(1.22)> CoZr(1.17)>$Co_3O_4$(0.72), which implied the potential of excellent redox ability on Pt-supported catalysts. The $H_2$-TPR experiment was employed to further determined the effect of Pt addition on the redox property. As showed in Fig. 4d, two clear reduction peaks at 348 °C and 439 °C were observed for the single $Co_3O_4$ catalyst, which were divided into two stages of $Co^{3+}$ to $Co^{2+}$ and $Co^{2+}$ to Co, particularly [15,37]. After the introduction of Pt, the reduction peaks of Co shifted to lower temperature. Meanwhile, the peaks around 100 °C were observed on 0.5 %Pt-CoZr and 0.5 %Pt-$Co_3O_4$, which were attributed to the reduction of the $PtO_x$ species [26]. And the $H_2$ consumption at temperatures below 200°C was significantly increased (Table S3), which was attributed to the weaken interaction between $PtO_x$ and $Co_3O_4$ [38]. These results demonstrated that Pt addition markedly improved the low-temperature redox activity of catalysts.

The XPS results of O 1 s highlighted the effects of Zr doping. As displayed in Fig. 4b and Fig. S9, three peaks at 529.6 eV, 531.1 eV and 532.20 eV were assigned to lattice oxygen ($O_{latt}$), surface-active oxygen ($O_{surf}$) and hydroxyl oxygen ($O_{OH}$), respectively [9]. Compared with the $Co_3O_4$ catalyst, the binding energies of $O_{surf}$ peaks on CoZr significantly shifted to lower values. This indicated that the electron shifted towards oxygen sites, thereby enhancing the formation of $O_{surf}$ (such as $O_2^-$) on the catalyst surface [15]. As for 0.5 %Pt-$Co_3O_4$ and 0.5 %Pt-CoZr, the

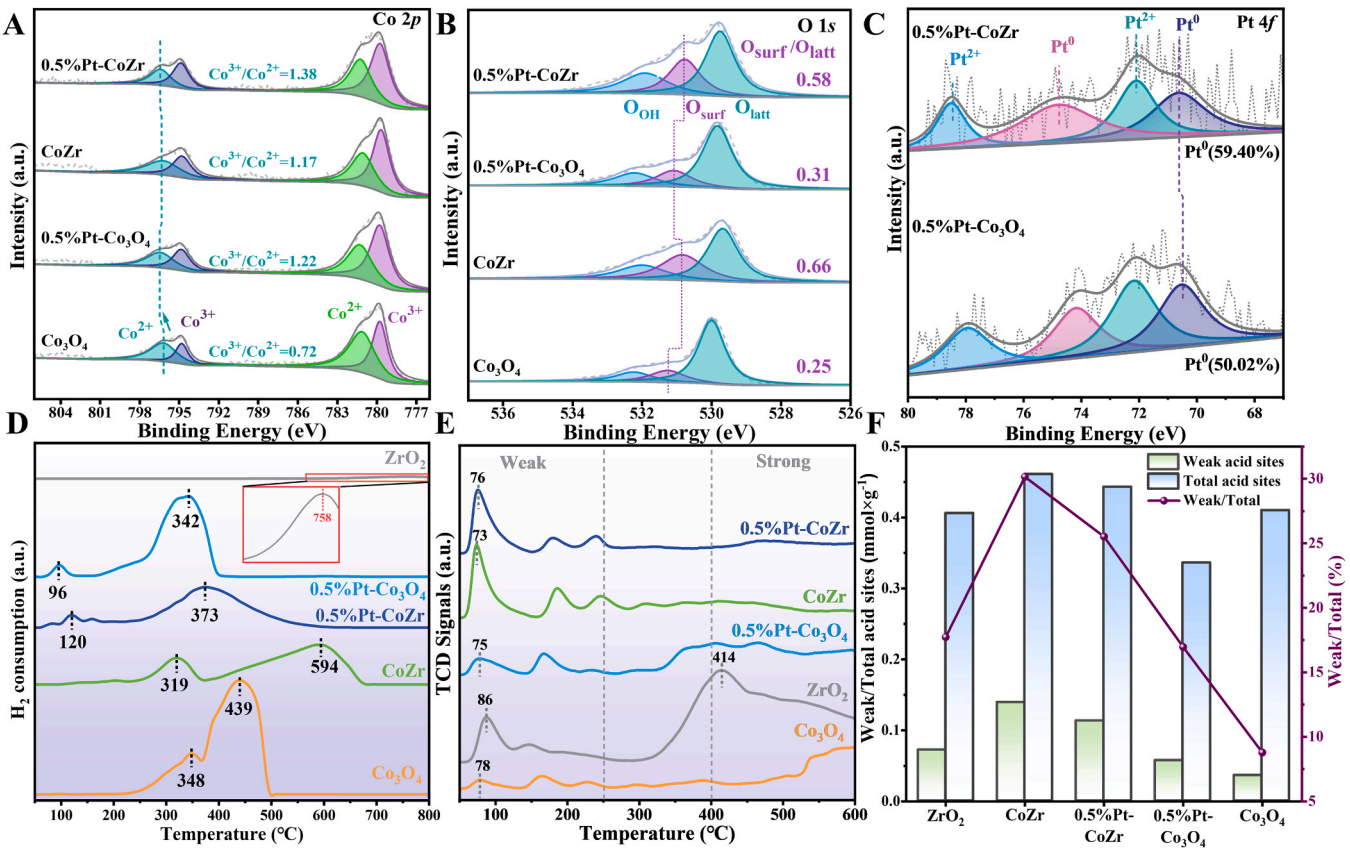


**Fig. 4.** XPS spectra of Co 2p(a), O 1 s(b) and Pt 4 f(c), $H_2$-TPR(d), $NH_3$-TPD(e) and acid sites of prepared catalysts(f).

chemical valences of the Pt species on these two catalysts were also studied by XPS. As shown in Fig. 4**c**, the peaks at 71.4 and 74.7 eV were related to the $Pt^0$ species, while the peaks at 72.5 and 75.8 eV were correlated with the $Pt^{2+}$ species [14]. Compared with 0.5 %Pt-$Co_3O_4$, after introducing Zr, an increased proportion of active $Pt^0$ species (59.40 %) was observed on the surface of 0.5 %Pt-CoZr, [39]. Simultaneously, the binding energy of $Pt^0$ shifted to higher values on 0.5 % Pt-CoZr, while the binding energy of $O_{surf}$ shifted to higher values in Fig. 4b. This demonstrated that Zr incorporation facilitated electron transfer from Pt to O on the 0.5 %Pt-CoZr surface, promoting the generation of more $O_2^-$. Furthermore, the higher ratio of $O_{surf}/O_{latt}$ were found on Zr-doped catalysts in Fig. 4b. Higher percentage of surface-active oxygen species implies more oxygen vacancies on the catalysts [33]. These results demonstrated that the introduction of Zr was conductive to regulate and improve the surface-active oxygen (e.g. $O_2^-$, $O^{2-}$) on prepared catalysts, which in turn accelerated the oxidation of ethane on 0.5 %Pt-CoZr.

Based on existing researches, metallic platinum ($Pt^0$) has been identified as one of the most reactive phases for the catalytic combustion of short-chain alkanes[40,41]. Further, it was considered that $Pt^0$ sites are conductive to activating $O_2$ to generate active oxygen and increasing the C-H and C-C activation ability of alkanes[42–45]. Besides, the increased percentages of $Pt^0$ species at higher binding energies was detected in 0.5 %Pt-CoZr catalysts compared to 0.5 %Pt-$Co_3O_4$, suggesting a significant interaction was formed between Pt and Zr. While putting the XPS results of Pt and Co into consideration together, the opposite change was detected due to the inner interactions. In detailed, higher percentages of high valence of Co ($Co^{3+}$) and low valence of Pt ($Pt^0$) were existed in 0.5 %Pt-CoZr, while the 0.5 %Pt-$Co_3O_4$ catalyst displayed reverse state. That is to say, electronic transfer must exist in these two metal elements. Thus, the higher percentages of active species ($Pt^0$, $Co^{3+}$and $O_{surf}$) jointly determined the activity of 0.5 %Pt-CoZr catalysts.

The surface acidity was reported to be beneficial to enhance the capacity of cracking the C-H bond and deep oxidation [26,46]. Here, temperature-programmed desorption of $NH_3$($NH_3$-TPD) was carried out to identify the surface acidity and acid amount of prepared catalysts, and the results were displayed in Fig. 4e and Table S3. The $NH_3$ desorption zones at below 250 °C, 250–400 °C, and above 400 °C were assigned to the desorption of $NH_3$ adsorbed on weak, medium strong and strong acid sites on the catalyst surface, respectively [47]. It was obvious that pure $ZrO_2$ catalyst owned more abundant acid sites than pure $Co_3O_4$ catalyst. Meanwhile, as concluded in Table S3 and Fig. 4f, the total acidity improved with the incorporation of Zr on CoZr catalysts. The introduction of Pt on 0.5 %Pt-$Co_3O_4$ catalyst also made promoting influence on the total acidity. However, the weak acidity was greatly enhanced by Zr addition. Moreover, it was worth noting that the surface weak acid sites in both of 0.5 %Pt-CoZr and CoZr catalysts were significantly enhanced. Considering their exclusive catalytic performances of sulfur-resistance, it could be proposed that the introduction of Zr enhanced the surface weak acidity and consequently strengthened the tolerance to sulfur, which corresponded to the previous work [48].

### 3.4. Reaction mechanism study

To get deep insights into the reaction mechanism, the $C_2H_6$ degradation processes were investigated by in situ DRIFTs on the 0.5 %Pt-CoZr catalyst. Firstly, the flow of 0.2 vol% $C_2H_6/N_2$ was introduced into the reaction chamber to reveal the adsorption of $C_2H_6$ at 150 °C. As displayed in Fig. 5a, the signal of bands at 2983, 2931 and 2894 $cm^{-1}$ were assigned to the C-H stretching vibrations of gaseous $C_2H_6$ [3,4]. Meanwhile, the band at 1436 $cm^{-1}$ corresponded to the ethyl was detected, and multiple bands attributed to the carbonate and carboxylate species were also observed at 1000–1600 $cm^{-1}$, which implied that

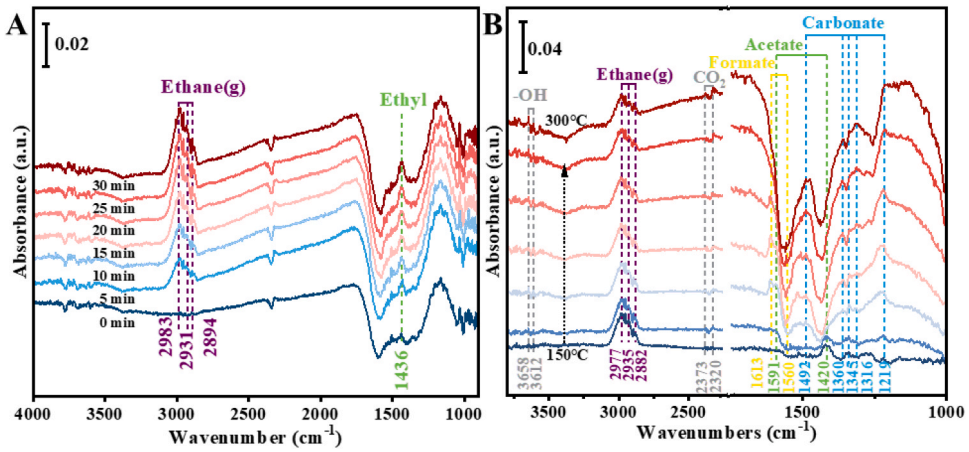


**Fig. 5.** In situ DRIFTS of ethane adsorption (a) and oxidation (b) over 0.5 %Pt-CoZr catalyst.

the broken of first C-H band happened owing to the surface-active oxygen of 0.5 %Pt-CoZr catalyst [49]. After reaching adsorption saturation within 30 min, the feed gas was replaced with 0.2 vol% $C_2H_6$ and air, and the reaction temperature was gradually increased. As displayed in Fig. 5b, the bands intensity of ethane on the 0.5 %Pt-CoZr catalyst gradually declined and the bands of hydroxyl species (3658 and 3612 $cm^{-1}$) emerged with the progress of the oxidation reaction [50]. At the low temperature, the peaks at 1420 $cm^{-1}$ ($CH_3CHOOH$) and 1345 $cm^{-1}$ (polydentate carbonate) were firstly found [33,51]. With the increasing of the temperature, the peaks of formate (1560 and 1613 $cm^{-1}$) and acetate (1591 $cm^{-1}$) emerged and then disappeared [38,52]. Besides, the carbonate species (1219, 1316, 1360 and 1492 $cm^{-1}$) were always the dominant intermediates during the $C_2H_6$ degradation [36,53]. Moreover, the detailed peaks of the intermediates at 1650–1200 $cm^{-1}$ were shown in Fig. S12. Based on the above results, the degradation path of $C_2H_6$ oxidation was proposed as followed by: $CH_3CH_3 \rightarrow CH_3CH_2^* \rightarrow CH_3HCOO^* \rightarrow HCOO^* \rightarrow HCO_3^*/CO_3^* \rightarrow H_2O$ and $CO_2$, which obeyed the MvK mechanisms. It was worth noting that during the reaction of ethane on the CoZr surface, the signal peaks of acetate and carbonate were observed, while no obvious formate signal

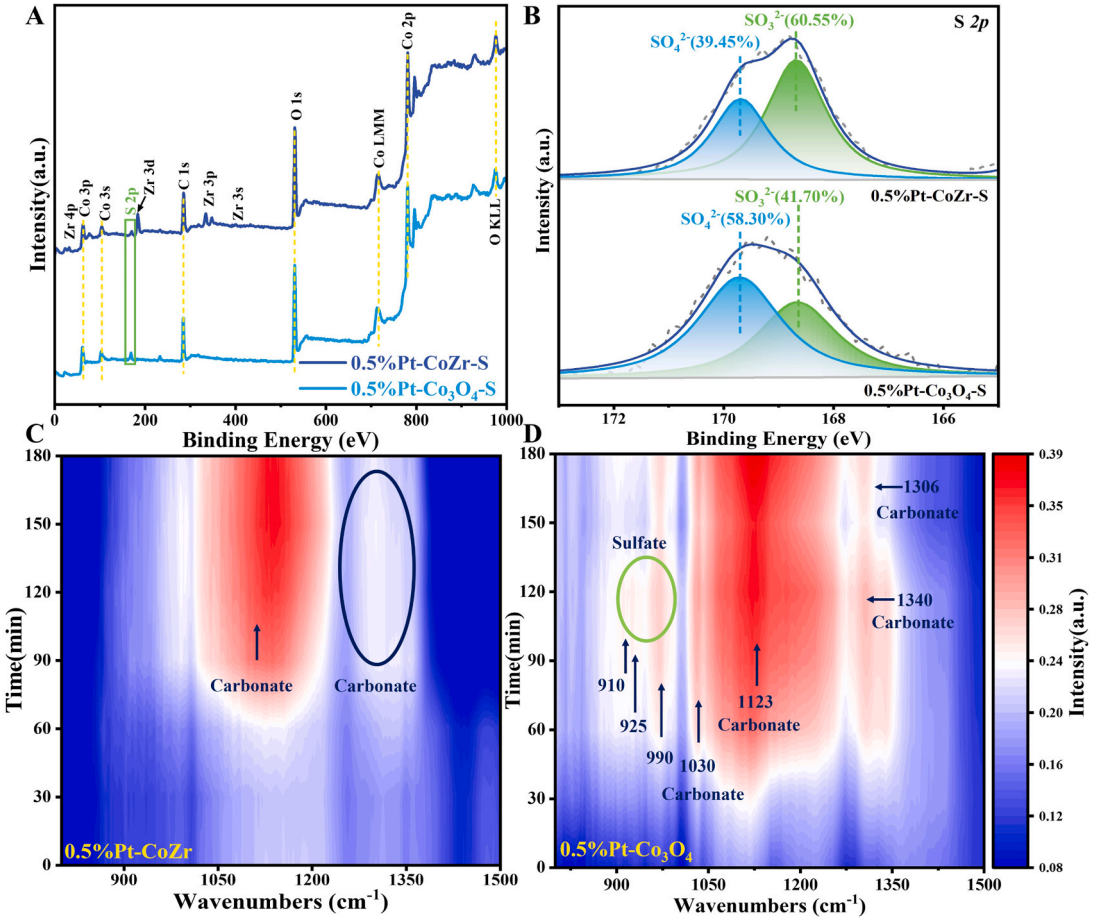


**Fig. 6.** XPS survey spectra (a); and S 2p spectra (b) of used catalysts under long-time exposure of $SO_2$; time-resolved in situ DRIFTS spectra collected at 275 °C under $SO_2$ exposure over 0.5 %Pt-CoZr (c) and 0.5 %Pt-$Co_3O_4$ (d) catalysts (2000 $C_2H_6$, 50 ppm $SO_2$, and 21 % $O_2$).

peak was detected (Fig. S10). However, after the introduction of Pt, a significant formate signal peak was observed on the 0.5 %Pt-CoZr surface. These results indicated that on the CoZr surface, the catalytic reaction of ethane only proceeded to the C-H bond cleavage stage, whereas the presence of Pt on the 0.5 %Pt-CoZr surface facilitated C-C bond cleavage and promoted the conversion of acetate to formate.

The results in Fig. 1f demonstrated that the introduction of Zr could significantly enhance the sulfur resistance of the catalyst. To distinguish the effects of Zr modification on the enhancement of the sulfur resistance, the distribution and chemical states of S species on the surfaces of used 0.5 % Pt-CoZr and 0.5 % Pt-$Co_3O_4$ were analyzed. XPS survey spectra of 0.5 %Pt-CoZr-S and 0.5 %Pt-$Co_3O_4$-S (after 480-min ethane oxidation reaction with $SO_2$) were displayed in Fig. 6a. The peaks observed at 169.70 and 168.70 eV were correspond to $SO_4^{2-}$ and $SO_3^{2-}$ species, respectively [54]. And the higher percentage of stable sulfates was formed on the 0.5 %Pt-$Co_3O_4$-S catalyst (58.30 %) compared with 0.5 %Pt-CoZr-S (Table 2). Similarly, the percentage of S content in 0.5 % Pt-$Co_3O_4$-S surface was twice of that in 0.5 %Pt-CoZr-S surface, along with the increased contents of O element. This indicated that on the surface of 0.5 %Pt-$Co_3O_4$, $SO_2$ was more likely to consume surface active oxygen species to form sulfate deposits on the catalyst surface. After introducing Zr, the generation of sulfate on the surface of 0.5 %Pt-CoZr was significantly inhibited. This was mainly because the introduction of Zr increased the surface acidity of the 0.5 %Pt-CoZr catalyst (Fig. 4e), thereby inhibiting the adsorption of $SO_2$ [55].

In order to validate the effects of sulfates on ethane oxidation, we further carried out a 180-min continuous test of in situ DRIFTS under the condition of 0.2 vol% $C_2H_6$, 50 ppm $SO_2$ and air at 275 °C. As depicted in Fig. 6c and d, there were obvious bands of carbonate intermediates (1030, 1123,1360 and 1340 $cm^{-1}$) on the both catalysts [56,57]. However, the bands of sulfates (910, 925 and 990 $cm^{-1}$) gradually emerged and intensified within 60 min on the surface of the 0.5 % Pt-$Co_3O_4$ catalyst [58]. Meanwhile, the bands intensity of carbonates became higher as well. These phenomena indicated that $SO_2$ undergone oxygen-competitive reactions with ethane by consuming surface-active oxygen on 0.5 %Pt-$Co_3O_4$, resulting in the deposition of sulfates on the surface, which in turn hindered the deep degradation of ethane's reaction intermediates, such as carbonates. However, no evident bands of sulfates were detected on the 0.5 %Pt-CoZr catalyst. Therefore, it was reasonable to deduce that the modification of Zr could greatly prevent the accumulation and further conversion of sulfates in 0.5 %Pt-CoZr catalyst, which maintained the satisfactory performances under long-time exposure to $SO_2$ (Fig. 1f).

## 4. Discussion

Based on the above results, both Pt and Zr play crucial roles in the catalytic oxidation of ethane over the 0.5 %Pt-CoZr catalyst. The comprehensive relationship between structure and performance of catalysts was concluded in Fig. 7a. Specifically, the introduction of 0.5 % Pt significantly enhanced the ethane conversion rate of the catalyst. This was mainly because the introduction of Pt weakened the Co-O bond (Fig. 3d), facilitating the participation of O in the ethane oxidation process and the formation of corresponding oxygen vacancies (Fig. 3f). Additionally, the interaction between Pt and Co improves the low-temperature redox properties of the catalyst (Fig. 4d). Meanwhile, the increased $Co^{3+}/Co^{2+}$ ratio indicated that more electrons were transferred from Co to O, generating abundant surface-active oxygen species (e.g. $O^{2-}$, $O_2^-$), which promoted the deep degradation of ethane (Fig. 4b). As a co-catalyst, Zr also played an essential role in enhancing the ethane conversion. On the one hand, the introduction of Zr enhanced the specific surface area of the catalysts (Fig. 3b and c), facilitated the exposure of active sites, and offered reaction sites for ethane. Meanwhile, the presence of Zr enhanced the dispersion of Pt on the catalyst surface (Fig. 2). On the other hand, Zr regulated the surface electronic distribution, further promoting the generation of surface-active oxygen species (Fig. 4e). More importantly, the introduction of Zr enhanced the overall acidity of the catalyst, thereby inhibiting the adsorption of $SO_2$ and the deposition of sulfates on the catalyst surface (Fig. 6b).

The identification of key active sites in the catalytic oxidation of ethane is crucial. Through the analysis of the catalytic mechanisms of ethane on the 0.5 %Pt-CoZr surface, it was found that Pt served as the primary site for C-C bond cleavage, facilitating the decomposition of acetate into formate. In terms of sulfur resistance, $SO_2$ preferentially consumed active species on the 0.5 %Pt-$Co_3O_4$ surface, depositing sulfate species and inhibiting the deep degradation of key intermediates in ethane oxidation (Fig. 7b). However, the introduction of Zr significantly reduced the deposition of sulfate species on the 0.5 %Pt-CoZr surface. Ultimately, under the synergistic effects of Pt, Zr, and Co sites, ethane could be successfully and efficiently conversed into the harmless $CO_2$ and $H_2O$ under the exposure to $SO_2$ on the 0.5 %Pt-CoZr catalyst.

**Table 2**
XPS results of catalysts after long-time $SO_2$ exposure.

| Catalyst | Surface S content Atom.% | Surface O content Atom.% | Binding Energy (eV) | | $SO_4^{2-}$(%) |
|---|---|---|---|---|---|
| | | | $SO_4^{2-}$ | $SO_3^{2-}$ | |
| 0.5 %Pt-CoZr-S | 2.18 | 41.26 | 169.69 | 168.70 | 39.45 |
| 0.5 %Pt-$Co_3O_4$-S | 4.39 | 44.18 | 169.71 | 168.66 | 58.30 |

## 5. Conclusions

In summary, a series of $Co_xZr_{10-x}$ mixed oxides and Pt-supported catalysts were prepared for efficient ethane catalytic degradation under different conditions. The 0.5 %Pt-CoZr catalyst was the optimal candidate and achieved efficient performances with the $T_{90}$ of ethane oxidation at 247 °C. Moreover, great thermal stability and water resistance of 0.5 %Pt-CoZr catalyst were tested under 40-hour tests, demonstrating shining adaptability to variable working conditions. It was found that the interaction between Pt and Co critically contributed to the efficient catalytic performances. More oxygen vacancies and surface-active oxygen were obtained with the presence of Pt, implying the superior ability of activating the strong C-C bond in ethane. Compared to the CoZr catalyst, the introduction of Pt in 0.5 %Pt-CoZr catalyst promoted the conversion of intermediate species, especially the acetate. Meanwhile, the 0.5 %Pt-CoZr catalyst could maintain high activity after 480 min exposure to $SO_2$, while the 0.5 %Pt-$Co_3O_4$ catalyst was seriously poisoned within 240 min. Notably, the strengthened weak acid sites by Zr doping played the decisive role, which effectively inhibited the $SO_2$ adsorption and sulfates deposition. Besides, the Zr introduction was favorable to increase the specific surface area of catalysts and then promote the homogeneous distribution of Pt particles. Additionally, the results of in situ DRIFTs illustrated that the path of ethane oxidation was followed by $CH_3CH_3 \rightarrow CH_3CH_2^* \rightarrow CH_3HCOO^* \rightarrow HCOO^* \rightarrow HCO_3^*/CO_3^* \rightarrow H_2O$ and $CO_2$. Overall, this study proposed a satisfactory catalyst in efficient degradation of ethane under $SO_2$ exposure and provided an insight to eliminate short-chain alkanes emission.

## CRediT authorship contribution statement

**Ling Wang:** Writing – original draft, Investigation, Formal analysis, Data curation. **Beilong Lin:** Data curation, Conceptualization. **Shengyong Lu:** Supervision, Funding acquisition. **Jianhua Yan:** Supervision. **Zhiyuan Gong:** Methodology, Investigation. **Minghui Tang:** Writing – review & editing, Funding acquisition, Conceptualization.

## Declaration of Competing Interest

The authors declare the following financial interests/personal

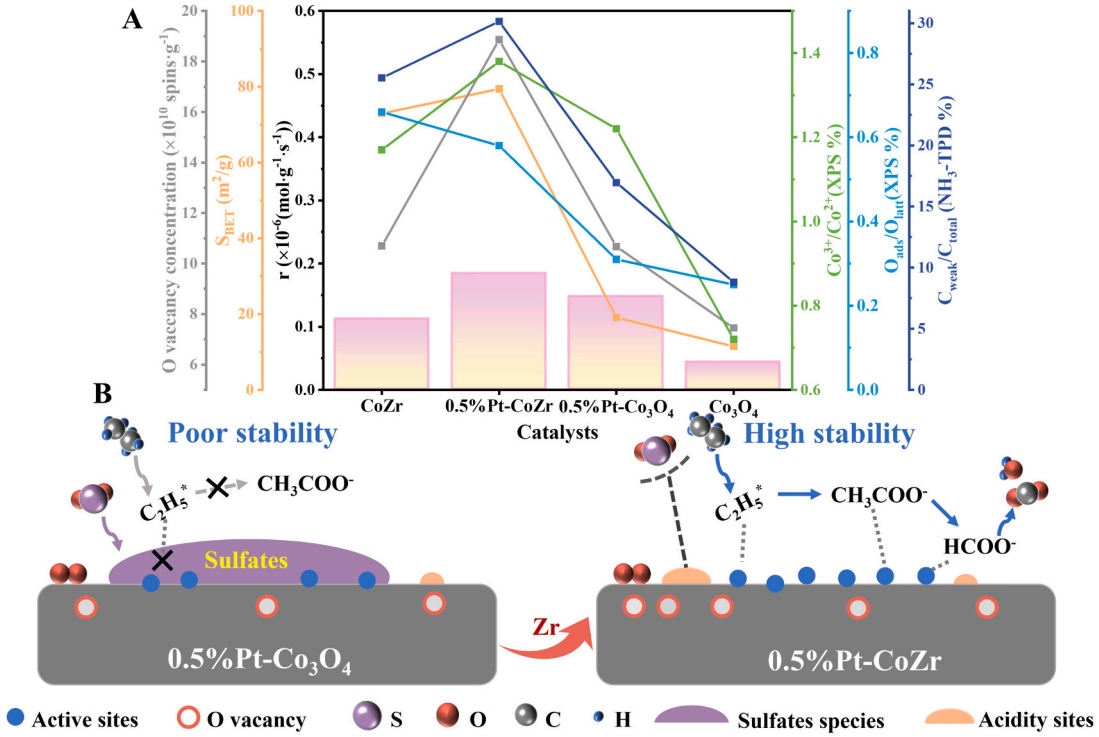


**Fig. 7.** Profiles for prepared catalysts, the relationship between reaction rate and $S_{BET}$, oxygen vacancy concentration surface $Co^{3+}/Co^{2+}$ ratio, $O_{surf}/O_{latt}$ ratio, and surface acidity(a), Catalytic pathway of ethane combustion over 0.5 %Pt-$Co_3O_4$ and 0.5 %Pt-CoZr catalysts in the presence $SO_2$(b).

relationships which may be considered as potential competing interests: Minghui Tang reports financial support was provided by National Key R&D Program of China (2022YFB4101500). Reports a relationship with that includes:. Has patent pending to. If there are other authors, they declare that they have no known competing financial interests or personal relationships that could have appeared to influence the work reported in this paper

## Acknowledgments

This investigation was financially supported by the National Key R&D Program of China (2022YFB4101500) and the "Pioneer" and "Leading Goose" R&D Program of Zhejiang (2023C03125).

## Appendix A. Supporting information

Supplementary data associated with this article can be found in the online version at doi:10.1016/j.jece.2025.118347.

## Data availability

Data will be made available on request.

## References

[1] C. He, J. Cheng, X. Zhang, M. Douthwaite, S. Pattisson, Z. Hao, Recent advances in the catalytic oxidation of volatile organic compounds: a review based on pollutant sorts and sources, Chem. Rev. 119 (2019) 4471–4568, https://doi.org/10.1021/acs.chemrev.8b00408.

[2] X. Yang, Q. Li, E. Lu, Z. Wang, X. Gong, Z. Yu, Y. Guo, L. Wang, Y. Guo, W. Zhan, J. Zhang, S. Dai, Taming the stability of Pd active phases through a compartmentalizing strategy toward nanostructured catalyst supports, Nat. Commun. 10 (2019) 1611, https://doi.org/10.1038/s41467-019-09662-4.

[3] S. Liu, H. Wang, S. Wang, Y. Dai, B. Liu, Y. Liu, F. Dang, K.J. Smith, X. Nie, S. Hou, X. Guo, Engineering morphology and Ni substitution of NixCo3–xO4 spinel oxides to promote catalytic combustion of ethane: elucidating the influence of oxygen defects, ACS Catal. 13 (2023) 4683–4699, https://doi.org/10.1021/acscatal.3c00286.

[4] Y. Jian, T. Yu, Z. Jiang, Y. Yu, M. Douthwaite, J. Liu, R. Albilali, C. He, In-depth understanding of the morphology effect of α-Fe2O3 on catalytic ethane destruction, ACS Appl. Mater. Interfaces 11 (2019) 11369–11383, https://doi.org/10.1021/acsami.8b21521.

[5] H. Zhang, Z. Wang, L. Wei, Y. Liu, H. Dai, J. Deng, Recent progress on VOC pollution control *via* the catalytic method, Chin. J. Catal. 61 (2024) 71–96, https://doi.org/10.1016/S1872-2067(24)60043-4.

[6] W. Tan, S. Xie, Y. Cai, H. Yu, K. Ye, M. Wang, W. Diao, L. Ma, S.N. Ehrlich, F. Gao, L. Dong, F. Liu, Surface lattice-embedded Pt single-atom catalyst on ceria-zirconia with superior catalytic performance for propane oxidation, Environ. Sci. Technol. 57 (2023) 12501–12512, https://doi.org/10.1021/acs.est.3c03497.

[7] A. Wang, J. Ding, M. Li, P. Song, Z. Zhao, Y. Guo, Y. Guo, L. Wang, Q. Dai, W. Zhan, Robust Ru/Ce@Co catalyst with an optimized support structure for propane oxidation, Environ. Sci. Technol. 58 (2024) 12742–12753, https://doi.org/10.1021/acs.est.4c03449.

[8] R. Fang, Y. Cui, Z. Shi, M. Gong, Y. Chen, Promotion of a Pd/Al2O3 close-coupled catalyst by Ni, Chin. J. Catal. 36 (2015) 994–1000, https://doi.org/10.1016/S1872-2067(15)60850-6.

[9] S. Song, M. Wen, W. Zhao, J. Kong, G. Li, T. An, Modulation mechanism of Mn-O strength in α-MnO2 catalyst for high-efficiency catalytic combustion of propane, Appl. Catal. B Environ. Energy 354 (2024) 124120, https://doi.org/10.1016/j.apcatb.2024.124120.

[10] Z. Hu, S. Qiu, Y. You, Y. Guo, Y. Guo, L. Wang, W. Zhan, G. Lu, Hydrothermal synthesis of NiCeOx nanosheets and its application to the total oxidation of propane, Appl. Catal. B Environ. 225 (2018) 110–120, https://doi.org/10.1016/j.apcatb.2017.08.068.

[11] J. Wang, D. Zhang, G. Zhao, D. Liu, A.T. Kuvarega, B.B. Mamba, J. Gui, Homogeneous CoCeOx nanocomposites with rich oxygen vacancies for effective catalytic oxidation of toluene, Sep. Purif. Technol. 320 (2023) 124130, https://doi.org/10.1016/j.seppur.2023.124130.

[12] R. Chen, T. Zhang, Y. Guo, J. Wang, J. Wei, Q. Yu, Recent advances in simultaneous removal of SO2 and NOx from exhaust gases: removal process, mechanism and kinetics, Chem. Eng. J. 420 (2021) 127588, https://doi.org/10.1016/j.cej.2020.127588.

[13] H. Zhang, T. Wang, Y. Zhang, J. Wang, B. Sun, W.-P. Pan, A review on adsorbent/catalyst application for mercury removal in flue gas: effect of sulphur oxides (SO2, SO3), J. Clean. Prod. 276 (2020) 124220, https://doi.org/10.1016/j.jclepro.2020.124220.

[14] W. Chen, J. Zheng, Y. Fang, Y. Wang, J. Hu, Y. Zhu, X. Zhu, W. Li, Q. Zhang, C. Pan, B. Zhang, X. Qiu, S. Wang, S. Cui, J. Wang, J. Wu, Z. Luo, Y. Guo, Role of the in-situ-formed surface (Pt–S–O)-Ti active structure in SO2-promoted C3H8 combustion over a Pt/TiO2 catalyst, Environ. Sci. Technol. 58 (2024) 3041–3053, https://doi.org/10.1021/acs.est.3c08380.

[15] Y. Jian, Z. Jiang, M. Tian, M. Ma, L. Xia, S. Chai, J. Wang, R. Albilali, C. He, Low-temperature propane activation and mineralization over a Co3O4 sub-nanometer

porous sheet: atomic-level insights, JACS Au 3 (2023) 3076–3088, https://doi.org/10.1021/jacsau.3c00471.
[16] W. Zhang, J.L. Valverde, A. Giroir-Fendler, Co3O4-based catalysts for propane total oxidation: A state-of-the-art minireview, Appl. Catal. B Environ. 337 (2023) 122908, https://doi.org/10.1016/j.apcatb.2023.122908.
[17] X. Hao, J. Deng, Y. Liu, L. Jing, J. Wang, Z. Wang, H. Dai, Mesoporous NaxMnOy-supported platinum–cobalt bimetallic single-atom catalysts with good sulfur dioxide tolerance in propane oxidation, ACS Sustain. Chem. Eng. 10 (2022) 8326–8341, https://doi.org/10.1021/acssuschemeng.2c00932.
[18] Z. Zheng, S. Wu, Z. Huang, H. Xu, W. Shen, Insights into enhancing SO2 tolerance for catalytic combustion of toluene over sulfated CeZrOx supported platinum catalysts, Colloids Surf. A Physicochem. Eng. Asp. 669 (2023) 131539, https://doi.org/10.1016/j.colsurfa.2023.131539.
[19] L. Zhong, Q. Fang, X. Li, Q. Li, C. Zhang, G. Chen, SO2 resistance of Mn–Ce catalysts for lean methane combustion: effect of the preparation method, Catal. Lett. 149 (2019) 3268–3278, https://doi.org/10.1007/s10562-019-02896-3.
[20] L. Jiang, Q. Liu, G. Ran, M. Kong, S. Ren, J. Yang, J. Li, V2O5-modified Mn-Ce/AC catalyst with high SO2 tolerance for low-temperature NH3-SCR of NO, Chem. Eng. J. 370 (2019) 810–821, https://doi.org/10.1016/j.cej.2019.03.225.
[21] K. Zha, S. Wu, Z. Zheng, Z. Huang, H. Xu, W. Shen, Insights into boosting SO2 tolerance for catalytic oxidation of propane over Fe2O3-promoted Co3O4/halloysite catalysts, Ind. Eng. Chem. Res. 61 (2022) 12482–12492, https://doi.org/10.1021/acs.iecr.2c01902.
[22] X. Zheng, Y. Li, S. Liang, Z. Yao, Y. Zheng, L. Shen, Y. Xiao, Y. Zhang, C. Au, L. Jiang, Promoting effect of Cu-doping on catalytic activity and SO2 resistance of porous CeO2 nanorods for H2S selective oxidation, J. Catal. 389 (2020) 382–399, https://doi.org/10.1016/j.jcat.2020.06.010.
[23] L. Yang, P. Wang, L. Yao, X. Meng, C.Q. Jia, X. Jiang, W. Jiang, Copper doping promotion on Ce/CAC-CNT catalysts with high sulfur dioxide tolerance for low-temperature $NH_3$ –SCR, ACS Sustain. Chem. Eng. 9 (2021) 987–997, https://doi.org/10.1021/acssuschemeng.0c08490.
[24] L. Kang, L. Han, P. Wang, C. Feng, J. Zhang, T. Yan, J. Deng, L. Shi, D. Zhang, $SO_2$ -tolerant NO $_x$ reduction by marvelously suppressing $SO_2$ adsorption over $Fe_\delta Ce_{1-\delta} VO_4$ catalysts, Environ. Sci. Technol. 54 (2020) 14066–14075, https://doi.org/10.1021/acs.est.0c05038.
[25] S. Wu, C. Feng, F. Dong, S. Ma, W. Han, W. Han, H. Zhang, Z. Tang, Tailored CoNiOx@CuVOx core-shell catalyst exhibiting strong charge transfer and SO2 tolerance for efficient elimination of propane, Appl. Catal. B Environ. Energy 372 (2025) 125293, https://doi.org/10.1016/j.apcatb.2025.125293.
[26] C. Shao, Y. Cui, L. Zhang, J. Tang, C. Ge, B. Chen, L. Wang, Y. Guo, W. Zhan, Y. Guo, Boosting propane purification on Pt/ZrOSO4 nanoflowers: insight into the roles of different sulfate species in synergy with Pt, Sep. Purif. Technol. 304 (2023) 122367, https://doi.org/10.1016/j.seppur.2022.122367.
[27] Y. Ding, Q. Wu, B. Lin, Y. Guo, Y. Guo, Y. Wang, L. Wang, W. Zhan, Superior catalytic activity of a Pd catalyst in methane combustion by fine-tuning the phase of ceria-zirconia support, Appl. Catal. B Environ. 266 (2020) 118631, https://doi.org/10.1016/j.apcatb.2020.118631.
[28] G. Chai, W. Zhang, L.F. Liotta, M. Li, Y. Guo, A. Giroir-Fendler, Total oxidation of propane over Co3O4-based catalysts: elucidating the influence of Zr dopant, Appl. Catal. B Environ. 298 (2021) 120606, https://doi.org/10.1016/j.apcatb.2021.120606.
[29] K. Zeng, X. Li, C. Wang, Z. Wang, P. Guo, J. Yu, C. Zhang, X.S. Zhao, Three-dimensionally macroporous MnZrOx catalysts for propane combustion: synergistic structure and doping effects on physicochemical and catalytic properties, J. Colloid Interface Sci. 572 (2020) 281–296, https://doi.org/10.1016/j.jcis.2020.03.093.
[30] S. Wu, H. Liu, Z. Huang, H. Xu, W. Shen, Mn1ZrxOy mixed oxides with abundant oxygen vacancies for propane catalytic oxidation: Insights into the contribution of Zr doping, Chem. Eng. J. 452 (2023) 139341, https://doi.org/10.1016/j.cej.2022.139341.
[31] S. He, J. Guo, X. Liu, J. Liang, H. Zhang, Y. Deng, Zr doped La-Mn perovskite oxides: NH3–SCR activity, resistance to SO2/H2O and deactivation mechanism, Fuel 371 (2024) 131846, https://doi.org/10.1016/j.fuel.2024.131846.
[32] G. Li, N. Li, Y. Sun, Y. Qu, Z. Jiang, Z. Zhao, Z. Zhang, J. Cheng, Z. Hao, Efficient defect engineering in Co-Mn binary oxides for low-temperature propane oxidation, Appl. Catal. B Environ. 282 (2021) 119512, https://doi.org/10.1016/j.apcatb.2020.119512.
[33] F. Dang, Z. Jiang, Y. Wang, J. Wan, C. Ai, M. Tian, Y. Jian, H. Xu, R. Albilali, J. Yu, C. He, Enhanced light alkane oxidation under impurity-containing conditions by low-coordinated Co–O structures boosting C–H bond activation, ACS Catal. 14 (2024) 14031–14042, https://doi.org/10.1021/acscatal.4c03638.
[34] W. Zhang, C. Descorme, J.L. Valverde, A. Giroir-Fendler, Yttrium-modified Co3O4 as efficient catalysts for toluene and propane combustion: effect of yttrium content, J. Hazard. Mater. 437 (2022) 129316, https://doi.org/10.1016/j.jhazmat.2022.129316.
[35] M. Zhang, X. Sui, X. Zhang, M. Niu, C. Li, H. Wan, Z.-A. Qiao, H. Xie, X. Li, Multi-defects engineering of NiCo2O4 for catalytic propane oxidation, Appl. Surf. Sci. 600 (2022) 154040, https://doi.org/10.1016/j.apsusc.2022.154040.
[36] G. Li, K. He, F. Zhang, G. Jiang, Z. Zhao, Z. Zhang, J. Cheng, Z. Hao, Defect enhanced CoMnNiOx catalysts derived from spent ternary lithium-ion batteries for low-temperature propane oxidation, Appl. Catal. B Environ. 309 (2022) 121231, https://doi.org/10.1016/j.apcatb.2022.121231.
[37] Z. Ren, Z. Wu, W. Song, W. Xiao, Y. Guo, J. Ding, S.L. Suib, P.-X. Gao, Low temperature propane oxidation over Co3O4 based nano-array catalysts: Ni dopant effect, reaction mechanism and structural stability, Appl. Catal. B Environ. 180 (2016) 150–160, https://doi.org/10.1016/j.apcatb.2015.04.021.
[38] Z. Huang, S. Cao, J. Yu, X. Tang, Y. Guo, Y. Guo, L. Wang, S. Dai, W. Zhan, Total oxidation of light alkane over phosphate-modified Pt/CeO2 catalysts, Environ. Sci. Technol. 56 (2022) 9661–9671, https://doi.org/10.1021/acs.est.2c00135.
[39] Z. Huang, J. Ding, X. Yang, H. Liu, P. Song, Y. Guo, Y. Guo, L. Wang, W. Zhan, Highly efficient oxidation of propane at low temperature over a Pt-based catalyst by optimization support, Environ. Sci. Technol. 56 (2022) 17278–17287, https://doi.org/10.1021/acs.est.2c05599.
[40] H. Hao, B. Jin, W. Liu, X. Wu, F. Yin, S. Liu, Robust Pt@TiOx/TiO2 catalysts for hydrocarbon combustion: effects of Pt-TiOx interaction and sulfates, ACS Catal. 10 (2020) 13543–13548, https://doi.org/10.1021/acscatal.0c03984.
[41] Y.-R. Liu, X. Li, W.-M. Liao, A.-P. Jia, Y.-J. Wang, M.-F. Luo, J.-Q. Lu, Highly active Pt/BN catalysts for propane combustion: the roles of support and reactant-induced evolution of active sites, ACS Catal. 9 (2019) 1472–1481, https://doi.org/10.1021/acscatal.8b03666.
[42] Y. Dun, Y. Liu, J. Xu, L. Xie, C. Du, C. Wang, Y. Zhao, F. Liu, R. Chen, B. Shan, Pt0-MnSO4 active centers on modified SmMn2O5 mullite oxides for efficient propane oxidation, Appl. Catal. B Environ. Energy 371 (2025) 125223, https://doi.org/10.1016/j.apcatb.2025.125223.
[43] L.-Y. Xu, C.-H. Wen, X.-H. Luo, W.-X. Zhang, X. Zhao, Q.-H. Yang, J.-Q. Lu, M.-F. Luo, J. Chen, Regulating the synergy of sulfate and Pt species in Pt/ZSM-5 for propane complete oxidation, Appl. Catal. B Environ. Energy 354 (2024) 124135, https://doi.org/10.1016/j.apcatb.2024.124135.
[44] Y. Fang, H. Li, Q. Zhang, C. Wang, J. Xu, H. Shen, J. Yang, C. Pan, Y. Zhu, Z. Luo, Y. Guo, Oxygen vacancy-governed opposite catalytic performance for C3H6 and C3H8 combustion: the effect of the pt electronic structure and chemisorbed oxygen species, Environ. Sci. Technol. 56 (2022) 3245–3257, https://doi.org/10.1021/acs.est.1c07573.
[45] S. Ge, Y. Chen, X. Tang, Y. Shen, Y. Lou, L. Wang, Y. Guo, J. Llorca, Preformed Pt nanoparticles supported on nanoshaped CeO2 for total propane oxidation, ACS Appl. Nano Mater. 6 (2023) 15073–15084, https://doi.org/10.1021/acsanm.3c02688.
[46] W. Zhu, X. Chen, C. Li, Z. Liu, C. Liang, Manipulating morphology and surface engineering of spinel cobalt oxides to attain high catalytic performance for propane oxidation, J. Catal. 396 (2021) 179–191, https://doi.org/10.1016/j.jcat.2021.02.014.
[47] G. Mu, H. Xie, Y. Jian, Z. Jiang, L. Li, M. Tian, L. Zhang, J. Wang, S. Chai, C. He, Facile construction and enhanced catalytic activity of Co-Mn oxide with rich amorphous/crystalline interfaces for propane oxidation, Sep. Purif. Technol. 348 (2024) 127699, https://doi.org/10.1016/j.seppur.2024.127699.
[48] C. Chen, Y. Wang, J. Li, F. Tian, W. Chen, C. Feng, Y. Pan, Y. Liu, In situ construction of heteroatom F-doped Mn3O4 spinel catalysts with robust activity and SO2 resistance for NH3-SCR at low temperature, Appl. Catal. B Environ. 338 (2023) 123086, https://doi.org/10.1016/j.apcatb.2023.123086.
[49] Y. Liu, H. Hu, J. Zheng, F. Xie, H. Gu, S. Rostamnia, F. Pan, X. Liu, L. Zhang, Interfacial engineering enables surface lattice oxygen activation of SmMn2O5 for catalytic propane combustion, Appl. Catal. B Environ. 330 (2023) 122649, https://doi.org/10.1016/j.apcatb.2023.122649.
[50] L. Xia, Y. Jian, Q. Liu, Y. Liu, J. Wang, S. Chai, M. Jing, R. Albilali, C. He, Boosted light alkane deep oxidation via metal bond length modulation-induced C–C bond preferential activation, Environ. Sci. Technol. 58 (2024) 3472–3482, https://doi.org/10.1021/acs.est.3c06916.
[51] L. Sun, X. Liang, H. Liu, H. Cao, X. Liu, Y. Jin, X. Li, S. Chen, X. Wu, Activation of Co-O bond in (110) facet exposed Co3O4 by Cu doping for the boost of propane catalytic oxidation, J. Hazard. Mater. 452 (2023) 131319, https://doi.org/10.1016/j.jhazmat.2023.131319.
[52] L. Xia, S. Xu, Y. Jian, X. Feng, Z. Jiang, J. Wang, Y. Li, Y. Wang, S. Chai, Y. Liu, H. Peng, R. Albilali, C. He, Efficient propane mineralization over unsaturated Pd cluster/CeO2 with prominent C-C cleavage capacity driven by inherent oxygen activation ability, J. Hazard. Mater. 461 (2024) 132509, https://doi.org/10.1016/j.jhazmat.2023.132509.
[53] C. Feng, Y. Wang, C. Chen, X. Fu, Y. Pan, H. Xin, Z. Wang, Y. Lu, X. Li, R. Zhang, Y. Liu, Fabrication of highly dispersed Pd-Mn3O4 catalyst for efficient catalytic propane total oxidation, J. Colloid Interface Sci. 650 (2023) 1415–1423, https://doi.org/10.1016/j.jcis.2023.07.076.
[54] B. Zhang, Y. Yang, J. Zheng, D. Zhang, W. Chen, W. Yuan, X. Chen, R. Liu, B. Chen, L. Li, L. Shi, J. Wang, Z. Luo, Y. Guo, Diverse effects of SO2-induced Pt–O–SO3 on the catalytic oxidation of C3H6 and C3H8, Environ. Sci. Technol. 58 (2024) 18020–18032, https://doi.org/10.1021/acs.est.4c04946.
[55] Y. Cai, B. Zhang, H. Yu, X. Ji, J. Sun, X. Wang, Q. Qian, L. Li, A. Liu, W. Tan, F. Gao, L. Dong, Shielding ceria based catalysts from SO2 poisoning in NH3-SCR reaction: modification effect of acid metal oxides, Appl. Catal. B Environ. 342 (2024) 123424, https://doi.org/10.1016/j.apcatb.2023.123424.
[56] Y. Fang, H. Li, Q. Zhang, C. Wang, J. Xu, H. Shen, J. Yang, C. Pan, Y. Zhu, Z. Luo, Y. Guo, Oxygen vacancy-governed opposite catalytic performance for $C_3H_6$ and $C_3H_8$ combustion: the effect of the Pt electronic structure and chemisorbed oxygen species, Environ. Sci. Technol. 56 (2022) 3245–3257, https://doi.org/10.1021/acs.est.1c07573.
[57] W. Zhu, Y. Li, H. Liu, Y. Yan, C. Liang, Boosting catalytic oxidation of propane over CeO2-supported Co3O4 catalyst with strong interfacial interaction and electron transfer, J. Catal. 434 (2024) 115529, https://doi.org/10.1016/j.jcat.2024.115529.
[58] R. Yin, J. Chen, L. Shan, J. Shi, K. Yang, H. Liu, J. Li, Prominent difference in the deactivation rate and mechanism of V2O5/TiO2 under H2S or SO2 during selective catalytic reduction of NOx with NH3, Appl. Catal. B Environ. 328 (2023) 122529, https://doi.org/10.1016/j.apcatb.2023.122529.